Prediction of the thermophysical properties of pure neon, pure argon, and the binary mixtures neon-argon and argon-krypton by Monte Carlo simulation using *ab initio* potentials

A. E. Nasrabad, R. Laghaei, and U. K. Deiters
Institute of Physical Chemistry, University of Cologne, Luxemburger Strasse 116, 50939 Koeln, Germany

(Received 20 January 2004; accepted 23 June 2004)

Gibbs ensemble Monte Carlo simulations were used to test the ability of intermolecular pair potentials derived *ab initio* from quantum mechanical principles, enhanced by Axilrod-Teller triple-dipole interactions, to predict the vapor-liquid phase equilibria of pure neon, pure argon, and the binary mixtures neon-argon and argon-krypton. The interaction potentials for Ne-Ne, Ar-Ar, Kr-Kr, and Ne-Ar were taken from literature; for Ar-Kr a different potential has been developed. In all cases the quantum mechanical calculations had been carried out with the coupled-cluster approach [CCSD(T) level of theory] and with correlation consistent basis sets; furthermore an extrapolation scheme had been applied to obtain the basis set limit of the interaction energies. The *ab initio* pair potentials as well as the thermodynamic data based on them are found to be in excellent agreement with experimental data; the only exception is neon. It is shown, however, that in this case the deviations can be quantitatively explained by quantum effects. The interaction potentials that have been developed permit quantitative predictions of high-pressure phase equilibria of noble-gas mixtures. © *2004 American Institute of Physics.* [DOI: 10.1063/1.1783271]

I. INTRODUCTION

For many years computer simulations have become an indispensable tool for the study of fluids. At first, such simulations aimed at single-phase properties only; the calculation of phase equilibria was not feasible for several reasons. But the introduction of efficient simulation techniques such as the Gibbs ensemble method[1] or Gibbs-Duhem integration[2] helped to overcome the obstacles, and over the previous years molecular simulations have thus become an important tool for the study of phase equilibria, too.[3]

Most molecular simulations, however, have been (and still are) carried out with ''model potentials'' (e.g., hard sphere, hard convex body, sphere+point multipole, etc.) or with simplified empirical potentials (e.g., OPLS). While the advantages of such potentials are evident (e.g., computational efficiency), there are also some drawbacks when such simulations are applied to real systems.

(1) The empirical potentials must be fitted to experimental data and are therefore usually valid in the same temperature and density range as these data only.

(2) The simulations are not predictive.

An approach for which the name ''global simulation'' had been coined decades ago, but which only recently has become feasible,[4–8] uses *ab initio* quantum mechanics to generate pair potentials, and then employs these in computer simulations to calculate thermodynamic properties of a given system. With modern computational resources it is now possible to calculate such interaction potentials for small- or medium-sized atoms and molecules with sufficient accuracy.

For strong intermolecular forces like hydrogen bonds, quantum mechanical calculations of pair interactions are already well established. The calculation of dispersion forces, however, is far more challenging, and it is necessary to apply past–self-consistent-field results to capture these interactions (for comprehensive reviews see Refs. 9 and 10).

It should be mentioned that there are even more fundamental approaches to the simulation of fluids, which even manage to avoid the construction of explicit pair potentials. At present, however, such approaches cannot account sufficiently well for electron correlation effects and hence for dispersion forces.

If such global calculations succeed, they yield thermodynamic data of fluids without any experimental input (except for the values of some universal constants). More specifically, it is no longer necessary to fit parameters to experimental data.

This is especially interesting for mixtures, because it is usually more difficult to find experimental data for mixtures than for pure components; and even if such data are available, it is more difficult to extract cross interaction potentials, cross virial coefficients, etc., from mixture data than to extract pure-component parameters from pure-component data.

One of the objectives of this work is to explore the feasibility of (fully predictive) global simulations of the phase equilibria of the noble-gas mixtures (neon+argon) and (argon+krypton). This implies the calculation of accurate *ab initio* potentials for the homonuclear dimers Ne_2, Ar_2, and Kr_2 as well as for the mixed dimers Ne-Ar and Ar-Kr.

Some of the required pair potentials are already available in the literature; some had to be calculated anew. This will be discussed in the following section. All *ab initio* pair potentials must be fitted to an appropriate analytical function before they can be used in computer simulations.

From previous work it is known that for quantitative agreement between simulations and experiments three-body

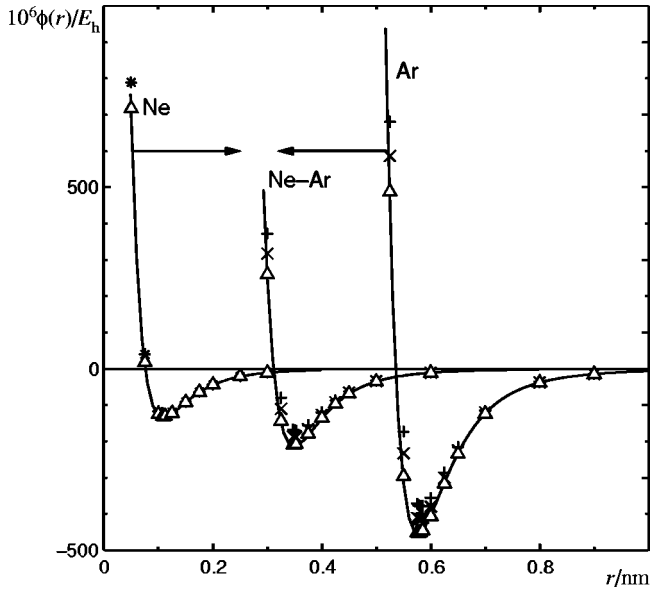

FIG. 1. Pair potentials neon-neon, neon-argon, and argon-argon. ——, experimental results (Refs. 13, 24, and 26); points, quantum mechanical results; +, avqz; ×, av5z; *, avtz+(332); △, extrapolation to basis set limit. For better visibility the curves of the pure components have been shifted outward by 0.2 nm; the arrows indicate the original location.

potentials have to be included. In the case of neon the importance of quantum corrections will be discussed.

II. INTERACTION POTENTIALS

In this work all energies and all parameters of pair potentials have been rendered dimensionless by multiplication by powers of the Hartree energy unit and the Bohr radius,

$$E_h = \frac{m_e e^4}{4h^2\epsilon_0^2} = 4.3597\times 10^{-18}\ \text{J},$$
$$a_0 = \frac{h^2\epsilon_0}{\pi m_e e^2} = 5.2918\times 10^{-11}\ \text{m}. \tag{1}$$

A. Neon

Cybulski and Toczyłowski[11] calculated *ab initio* potential energy curves for three homonuclear (He-He,Ne-Ne,Ar-Ar) and three heteronuclear (He-Ne,He-Ar,Ne-Ar) rare gas dimers using the CCSD(T) level of theory and several correlation consistent basis sets. In this work their results for the neon dimer obtained with the aug-cc-pVQZ (avqz) and aug-cc-pV5Z (av5z) basis sets were extrapolated towards the basis set limit of the interaction energies by means of the $1/X^3$ method;[12] the extrapolation result will be referred to as "av45z" in this work. The *ab initio* potentials resulting from the aug-cc-pVTZ+$(3s3p2d)$ [denoted here by avtz+(332)] and av45z basis sets, which were used in simulations, are shown in Fig. 1 and compared with the empirical potential of Aziz and Slaman.[13] It can be seen that the avtz+(332) potential is more repulsive than the empirical potential at short distances, and less attractive at and beyond the minimum, whereas the av45z potential shows an excellent agreement with the experimental data over the whole range of distances.

TABLE I. Characteristic properties of the neon-neon pair potentials. "MP4" denotes fourth order Møller-Plesset perturbation theory and "cc" coupled-cluster theory.

Potential	R_e/(Å)	$\epsilon/(10^{-6}E_h)$
cc/avtz+(332)[a]	3.114	125.83
cc/av5z+(33221)[a]	3.101	130.33
cc/av45z (this work)	3.097	130.95
MP4/av34z[b]	3.144	126.06
cc/NE2[d]		120.60
Experimental[c]	3.091	133.80

[a]Reference 11.
[b]Reference 15.
[c]Reference 12.
[d]Reference 5.

Numerical values for the two *ab initio* potentials have been provided in the supplementary material of this work.[14]

Leonhard and Deiters[15] developed another *ab initio* potential for the neon dimer using the MP4 level of theory and correlation consistent basis sets. They used the results of the avtz and avqz basis sets to extrapolate to the basis set limit. Table I shows the potential well depth ϵ and the well position R_e for the avtz+(332), av5z+(33221) (another basis set studied in Ref. 11), av45z, and MP4/av34z potentials and compares them with the corresponding values for the empirical potential of Aziz and Slaman.[13] It turns out that for the av45z potential the location of the well position is almost exact and the value of well depth is only about 2.1% less than the experimental value. The MP4 potential has a well depth 5.8% less than the empirical value, and the position of the minimum is shifted outward by 1.7%. For the avtz +(332) potential R_e and ϵ are 0.7% and 6.0% less than the corresponding values for the empirical potential. Even the best basis set,[11] av5z+(33221), does not give better results than the av45z extrapolation.

As computer simulations need analytical representation of the interaction potentials, the quantum mechanical results were fitted by a function proposed by Korona *et al.*[16] This function consists of a repulsive exponential component and an attractive damped dispersion component,

$$\phi(r) = Ae^{-\alpha r+\beta r^2} + \sum_{n=3}^{5} f_{2n}(r,b)\frac{C_{2n}}{r^{2n}}, \tag{2}$$

where A, α, β, and b denote adjustable parameters, the C_{2n} denote dispersion coefficients, and the f_{2n} are the damping functions of Tang and Toennies,[17]

$$f_{2n}(r,b) = 1 - e^{-br}\sum_{k=0}^{2n}\frac{(br)^k}{k!}. \tag{3}$$

Numerical values for the parameters are given in Table II.

We furthermore have to mention the *ab initio* potentials for neon by Garrison and Sandler[6] and Kirchner *et al.*,[5] which, however, do not match the empirical potential as well as the potentials mentioned above, and the work of Venkatraj *et al.*,[18] which was published after the completion of this work.

TABLE II. Parameters of neon-neon pair potentials [Eq. (2)].

Parameter	avtz+(332)	av45z
A/E_h	78.52	75.40
α/a_0^{-1}	2.133 71	2.167 74
β/a_0^{-2}	−0.035	−0.027
b/a_0^{-1}	1.88	1.86
$C_6/(E_h a_0^6)$	6.96	6.08
$C_8/(E_h a_0^8)$	49.87	114.08
$C_{10}/(E_h a_0^{10})$	2393.96	2008.32

The av45z potential was then used to calculate the second virial coefficient of neon from 20 up to 550 K using the equation

$$B(T) = -2\pi N_A \int_0^\infty \left[\exp\left(-\frac{\phi(r)}{k_B T} \right) - 1 \right] r^2 dr. \quad (4)$$

Here k_B denotes Boltzmann's constant, N_A Avogadro's constant, and T the temperature. Since for neon the influence of quantum effects is not negligible, the first terms of the quantum mechanical series expansion for $B(T)$ were added to the classical result of Eq. (4):[19]

$$\Delta B(T) = \Lambda^2 \frac{N_A}{12 k_B^2 T^2} \int_0^\infty \exp\left(-\frac{\phi(r)}{k_B T} \right) \left(\frac{d\phi(r)}{dr} \right)^2 r^2 dr - \Lambda^3 \frac{N_A}{4\sqrt{2}}. \quad (5)$$

Here Λ denotes the thermal de Broglie wavelength,

$$\Lambda = \frac{h}{\sqrt{2\pi m k_B T}}, \quad (6)$$

where m is the mass of a molecule. This correction term amounts to about +0.5 cm^3/mol at 100 K, and 3.5 cm^3/mol at 40 K. It can be seen in Fig. 3 that the calculated second virial coefficients agree well with the experimental data[20] except at very low temperatures, where the calculations as well as the experiments tend to be less reliable.

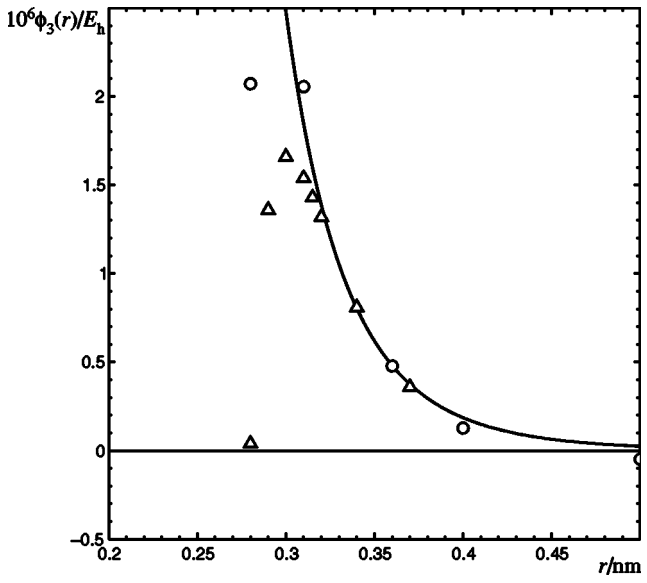

FIG. 2. Three-body potential of three neon atoms forming an equilateral triangle of side length r. Symbols, *ab initio* calculations; ○, Garrison and Sandler (Ref. 6); △, Ermakova *et al.* (Ref. 51); ——, Axilrod-Teller potential.

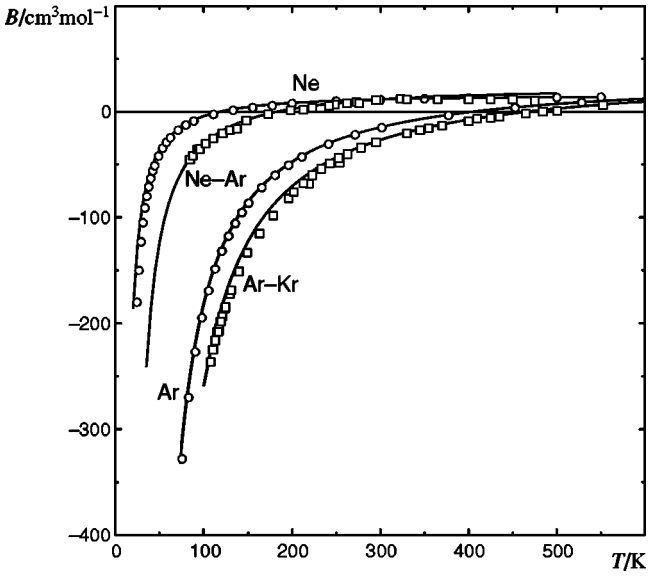

FIG. 3. Second virial coefficients of neon and argon, and cross second virial coefficients for neon-argon and argon-krypton. ——, predicted from *ab initio* pair potentials (after extrapolation to the basis set limit), ○; □, experimental data (Refs. 13, 24, and 26).

The Axilrod-Teller (AT) (Ref. 21) triple-dipole potential was used to account for three-body effects,

$$E_{AT} = \nu \frac{1 + 3\cos\alpha\cos\beta\cos\gamma}{r_{12}^3 r_{23}^3 r_{31}^3}, \quad (7)$$

where the r_{ik} are the lengths of the sides, and α, β, and γ are the angles of the triangle formed by three neon atoms. The value of the three-body nonadditivity coefficient ν that was used in the simulations is listed in Table VII.

The *ab initio* calculation of three-body potentials is a computationally demanding task and therefore not many attempts have been reported in the literature. A detailed analysis of the phenomenon by Bukowski and Szalewicz[22] in argon revealed that several nonadditivity effects tend to cancel out and that the remainder can be approximated by the AT potential. A similar view has been expressed by Malijevský and Malijevský.[23] For neon some *ab initio* calculations are shown in Fig. 2 and compared to the AT potential. It turns out that the AT function agrees well with the *ab initio* data at long distances; at very short distances it differs from the *ab initio* results—but then these differ from each other, too. Fortunately the distances for which the deviations become significant do not play a major rôle in computations for liquid neon.

We conclude that, in comparison to other sources of error, the deviations of the AT potential from *ab initio* values are not significant for the substances and the thermodynamic states studied in this work. This conclusion, however, should not be generalized. It has only been found to be valid in vapor-liquid equilibrium calculations for neon, argon, and—in previous publications—krypton and nitrogen; it may

TABLE III. Characteristic properties of the argon-argon pair potentials.

Potential	$R_e/(\text{Å})$	$\epsilon/(10^{-6}E_h)$
cc/av5z[a]	3.798	413.49
cc/av5z+(33221)[a]	3.779	441.90
cc/av45z	3.770	451.99
Experimental[b]	3.757	453.60

[a]Reference 11.
[b]Reference 24.

not be justified for other compounds, or in calculations of properties or thermodynamic states depending strongly on the short-distance part of the interaction potentials.

B. Argon

The calculation of high quality *ab initio* potentials for argon is more difficult than for neon, but still possible with the present-day computer resources. In this work we make use of the *ab initio* pair potentials of Cybulski and Toczylowski,[11] which had been obtained from coupled-cluster calculations at CCSD(T) level and with correlation consistent basis sets. In analogy to the case of neon, the results of two successive basis sets, avqz and av5z, were used to extrapolate to the basis set limit (referred to as av45z) of the interaction energies for argon by means of the $1/X^3$ extrapolation method. The results are shown in Table II of the supplementary material[14] as well as in Fig. 1; in the latter they are compared with the experimental potential of Aziz.[24] Evidently the av5z potential is too repulsive at short distances and not sufficiently attractive at large distances, whereas the av45z potential is in excellent agreement with the empirical potential over the whole range of intermolecular distances. The well depth and the location of the minimum of the *ab initio* potential as well as the empirical potentials are given in Table III. Surprisingly, these two properties are only 0.35% off the mark for the av45z potential, whereas the well depth of the av5z potential is too small by about 8.8%, and the distance of the minimum too small by 1.1%. The avqz potential yields even larger deviations from the experimental values.

Again Eq. (2) was used to fit the *ab initio* potential energy results obtained with the av45z basis set. The parameters are given in Table IV. The resulting pair potential was then used to predict the second virial coefficient of argon using relation (4). Figure 3 shows that the agreement with experimental data[25] is very good over the whole temperature range, confirming that the *ab initio* potential is indeed of high quality.

TABLE V. Characteristic properties of the neon-argon potentials. For the Berthelot-Lorentz combining rule (8) experimental potential parameters were used.

Potential	$R_e/\text{Å}$	$\epsilon/(10^{-6}E_h)$
cc/avqz[a]	3.548	170.95
cc/av5z[a]	3.518	188.65
cc/av5z+(33221)[a]	3.493	205.87
cc/av45z (this work)	3.490	208.61
Experimental[b]	3.489	214.05
Berthelot-Lorentz	3.424	246.36

[a]Reference 11.
[b]Reference 26.

C. Krypton

We recently developed an accurate *ab initio* pair potential for the krypton dimer,[8] using the same level of theory [CCSD(T)] and two correlation consistent basis sets, avtz and avqz, from which then an extrapolation to the basis set limit was made. The resulting pair potential was then fitted to Eq. (2). The parameters of the fit can be found in Table III of Ref. 8. The three-body nonadditivity coefficient of krypton is given in Table VII.

D. Neon-argon

In this work the cross pair potentials of neon-argon of Cybulski and Toczilowski[11] were used and again extrapolated towards the basis set limit with the $1/X^3$ extrapolation scheme. The resulting potentials are shown in Table III of the supplementary material[14] as well as in Fig. 1. For comparison the empirical potential of Barrow and Aziz[26] is shown in the figure, too.

As with the pure-component potentials, both the avqz and av5z potentials are much more repulsive at short distances and less attractive in the potential well and also in the dispersion portion of the potential function than the experimental potential, whereas the av45z potential shows a good agreement over the whole range of interatomic distances. Table V gives the characteristic properties of the *ab initio* potentials and compares them with experimental data. The distance of the minimum of the av45z potential turns out to be accurate and its well depth is too small by only 2.5%. For the avqz and av5z potentials the positions of the minimum

TABLE IV. Parameters of the argon-argon pair potential [Eq. (2)].

Parameter	av45z
A/E_h	56.21
α/a_0^{-1}	1.319 38
β/a_0^{-2}	−0.050
b/a_0^{-1}	1.70
$C_6/(E_h a_0^6)$	60.98
$C_8/(E_h a_0^8)$	1 941.02
$C_{10}/(E_h a_0^{10})$	62 960.00

TABLE VI. Parameters of the neon-argon pair potential [Eq. (2)].

Parameter	av45z
A/E_h	80.30
α/a_0^{-1}	1.8085
β/a_0^{-2}	−0.026
b/a_0^{-1}	1.70
$C_6/(E_h a_0^6)$	15.78
$C_8/(E_h a_0^8)$	563.00
$C_{10}/(E_h a_0^{10})$	21 460.00

TABLE VII. Three-body nonadditivity coefficients. The pure-component data of Anta *et al.* (Ref. 50) were used in this work.

	$\nu/(E_h a_0^9)$		
Interaction	Lit. (Ref. 50)	Eq. (9)	Lit. (Ref. 28)
Ne-Ne-Ne	12.02		11.95
Ne-Ne-Ar		42.13	40.49
Ne-Ar-Ar		147.63	142.50
Ar-Ar-Ar	517.40		518.30
Ar-Ar-Kr		746.5	744.6
Ar-Kr-Kr		1077.1	1074.0
Kr-Kr-Kr	1554.0		1572.0

are shifted outward by 1.7% and 0.8%, respectively, and the well depths are underestimated by 20.1% and 11.9%. These figures confirm that the $1/X^3$ extrapolation method is a good and efficient way to obtain the basis set limit, and that the av45z potentials are reliable.

In chemical engineering applications cross potential parameters are usually predicted from the Berthelot-Lorentz combining rules,

$$\epsilon_{12}=(1-k_{12})\sqrt{\epsilon_{11}\epsilon_{22}},$$

$$R_{e,12}=(1-l_{12})(R_{e,11}+R_{e,22})/2, \tag{8}$$

where k_{12} and l_{12} are adjustable parameters whose values are supposed to be close to zero. Table V shows that the R_e is almost additive; the combining rule predicts a value that is too small by 2%. For the energy parameter ϵ, however, Eq. (8) gives a result that is too high by 13%.

Again Eq. (2) was used to represent the quantum mechanical results analytically; the fitting parameters are given in Table VI.

The experimental determination of cross second virial coefficients is a difficult task, especially at low temperatures. Consequently, good experimental data are scarce in the literature. The av45z potential was used to calculate the cross second virial coefficients of neon-argon. The results are shown in Fig. 3 and compared with experimental data.[27] It can be seen that the calculated second virial coefficients are in good agreement with experiments at high temperatures; for lower temperatures the agreement deteriorates, but then the experimental uncertainty increases, too.

When the simulations included three-body potentials, the cross nonadditivity coefficients were estimated from the values of the pure-component coefficients,

$$\nu_{\text{Ne-Ne-Ar}}=\sqrt[3]{\nu_{\text{Ne}}\nu_{\text{Ne}}\nu_{\text{Ar}}},$$

$$\nu_{\text{Ne-Ar-Ar}}=\sqrt[3]{\nu_{\text{Ne}}\nu_{\text{Ar}}\nu_{\text{Ar}}}. \tag{9}$$

Table VII shows the three-body nonadditivity coefficients of the like and cross interactions, which were used in the simulations of neon-argon binary mixtures, along with those of Kumar and Meath.[28] For the noble gases, the geometrical mean rules (9) are indeed good approximations for these coefficients.

TABLE VIII. Characteristic properties of argon-krypton potentials.

Potential	σ/Å	R_e/Å	$\epsilon/(10^{-6}E_h)$
cc/avtz	3.6190	4.0475	371.80
cc/avqz	3.5425	3.9682	445.95
av34z	3.4868	3.9008	511.04
Experimental[a]	3.4640		525.06
Theory[b]	3.4570	3.8350	537.50
Berthelot-Lorentz	3.4599	3.8825	537.60

[a]Reference 30.
[b]Reference 31.

E. Argon-krypton

A pair potential for this atom pair has been calculated here by means of the GAUSSIAN® software, using the CCSD(T) method and two correlation consistent basis sets. Interaction energies were calculated at 14 different interatomic distances from 3.0 to 10.0 Å. The counterpoise method of Boys and Bernardi[29] was used to correct the basis set superposition error. The $1/X^3$ method was applied to estimate the basis set limit (av34z) of the interaction energies. Numerical results of the calculations for the *ab initio* potentials avtz, avqz, and av34z are presented in Ref. 14. Figure 4 shows that the av34z potential is less repulsive at short distances and also more attractive at and beyond the well minimum than the other two potentials.

For better comparison, the characteristic properties of the *ab initio* potentials avtz, avqz, and av34z are shown in Table VIII together with the empirical values of Kestin *et al.*[30] and also with predictions of McLure *et al.*[31] from a theory based on the nonconformality of intermolecular interactions, which gives accurate interaction potentials for simple fluids. Furthermore, the prediction from the

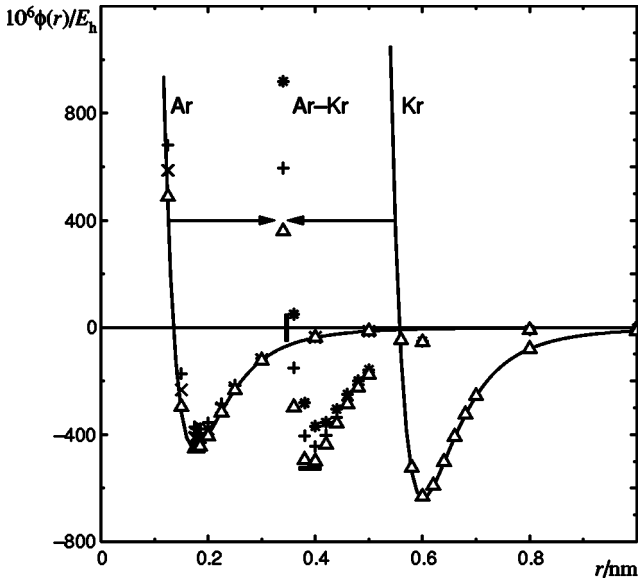

FIG. 4. Pair potentials argon-argon, argon-krypton, and krypton-krypton. ——, experimental results (Refs. 24 and 52); –, experimental minimum and zero location according to Ref. 30; points, quantum mechanical results:*, avtz; +, avqz; ×, av5z; △, extrapolation to basis set limit. For better visibility the curves of the pure components have been shifted outward by 0.2 nm; the arrows indicate the original location.

TABLE IX. Parameters of the argon-krypton pair potential [Eq. (2)].

Parameter	av34z
A/E_h	112.08
α/a_0^{-1}	1.422 41
β/a_0^{-2}	−0.040
b/a_0^{-1}	1.50
$C_6/(E_h a_0^6)$	94.08
$C_8/(E_h a_0^8)$	2 452.27
$C_{10}/(E_h a_0^{10})$	93 790.30

Berthelot-Lorentz rule (8) is shown. As in the case of the neon-argon potential, it turns out that the combining rules overestimate the depth of the cross pair potential. Only the quantum mechanical predictions come close to the experimental value.

The *ab initio* potentials are generally too repulsive: σ, the zero of the pair potential function for the avtz, avqz, and av34z potentials is 4.5%, 2.3%, and 0.7%, respectively, shifted outward in comparison with the experimental value.[30] The potential minima are shifted outward by 5.5%, 3.5%, and 1.7% in comparison with the result from nonconformal theory.[31] The deviations of the well depth are 28.5% for the avtz potential, 14.7% for avqz, and 2.7% for the extrapolation av34z. These figures show that the av34z is superior to the other *ab initio* potentials. Cross second virial coefficients calculated from this pair potential agree well with the experimental data,[32] as can be seen in Fig. 3.

Cross three-body potentials were estimated with Eq. (9). Table VII summarizes the nonadditivity coefficients for the like and mixed trimers and compares them with the values of Kumar and Meath.[28] As with the neon-argon system, the geometrical mean rule turns out to be a good approximation for cross nonadditivity coefficients. Fitting parameters for the av34z potential are given in Table IX.

III. SIMULATION DETAILS

Gibbs ensemble Monte Carlo (GEMC) simulations were used to calculate the thermodynamic properties of coexisting fluid phases of pure neon, pure argon, and binary mixtures neon-argon and argon-krypton. The simulations were performed with two-body as well as with two-body plus AT three-body potentials. For the pure component systems 5000 cycles were required to achieve equilibrium and further 5000 cycles to collect the averages; for binary mixtures the equilibration was slower and required 10 000 cycles.

A total number of 500 atoms for pure systems and 600–900 atoms for binary mixtures was distributed over two cubic simulation boxes with standard periodic boundary conditions and minimum image convention. Thermodynamic equilibrium conditions were fulfilled by executing the following trial moves: random particle displacements within each box (for thermal equilibrium), volume fluctuations of each box (for mechanical equilibrium), and particle transfer between the boxes (for material equilibrium). Each simulation cycle consisted of 500–900 trial particle displacements, one volume rearrangement for each box, and 50–1000 particle transfer attempts.

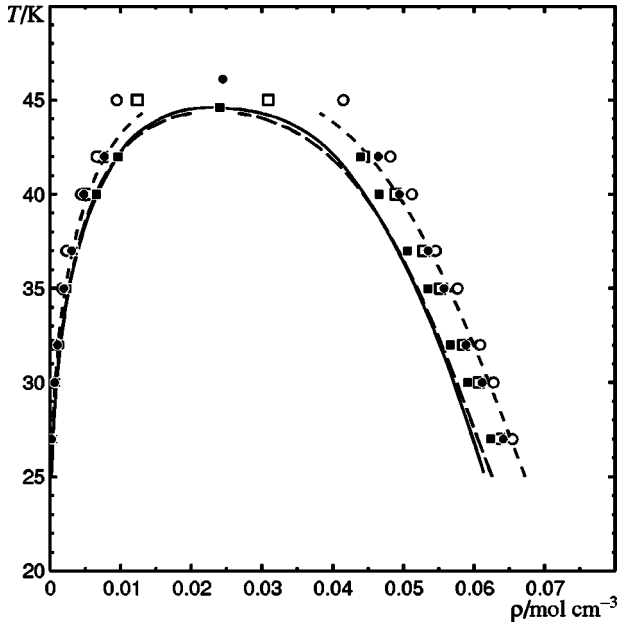

FIG. 5. Densities of coexisting phases of neon. ——, experimental data (Ref. 34); - - - -, uncorrected equation of state; — — —, equation of state with quantum correction. Points, GEMC computer simulation with the following interaction potentials: □, avtz+(332); ■, avtz+(332)+AT; ○, av45z; ●, av45z+AT.

The cutoff ratio for the two-body potential was equal to half the box length, and long-range corrections to the configurational energy were computed according to standard relations.[33] The cutoff ratio for the three-body potential was set to a quarter of the box length. Details of the three-body potential cutoff and the required long-range correction have been published previously.[15]

IV. RESULTS AND DISCUSSION

A. Neon

1. Simulation results

Simulations were performed along the vapor pressure curve from just above the triple point up to the critical region, using the av45z and avtz+(332) potentials with and without the AT three-body potential. Figures 5 and 6 show the predicted densities of coexisting phases and the vapor pressures together with the experimental data.[34] The results are also given numerically in the supplementary material (Tables V–VIII in Ref. 14). As the critical point cannot be obtained directly by computer simulations, a scaling law[35] was used to estimate the critical temperature,

$$\rho_l - \rho_g = b(T_c - T)^{\beta}, \tag{10}$$

where $\beta \approx 0.32$ is the nonclassical critical exponent; b and the critical temperature T_c were obtained by a least-squares fit to the (ρ, T) results with weights determined from the statistical uncertainty. The critical density ρ_c was then determined by a second fit from the law of rectilinear diameters,[35]

$$\frac{\rho_l + \rho_g}{2} = \rho_c + A(T - T_c). \tag{11}$$

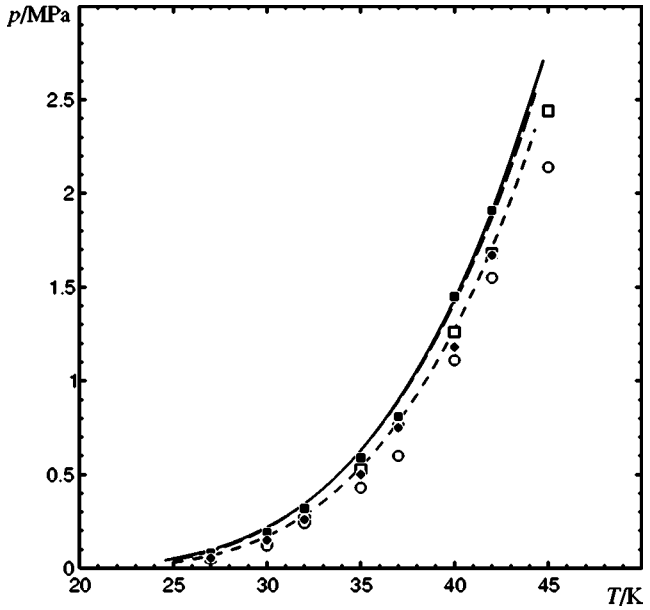

FIG. 6. Vapor pressure of neon. See Fig. 5 for an explanation of the symbols.

Table X shows the critical temperatures and densities for the various *ab initio* potentials as well as the experimental results.[36]

It can be seen in Figs. 5 and 6 that the inclusion of the AT potential significantly improves the simulation results obtained with the av45z potential. However, there are still large discrepancies between the simulation results and experimental data. The predicted critical temperature (46.10 K) and density (493.6 kg m^{-3}) for the av45z+AT potential are too large by 3.6% and 2.4%. The simulation results of the avtz +(332)+AT potential are quite satisfactory in the gas branch; the vapor pressure and also the predicted critical parameters are in excellent agreement with experiments, but there are still discrepancies in the liquid branch. The predicted critical temperature and density by the same simulations are only 0.25% and 0.58% above the experimental values, respectively. On the other hand, the simulation results obtained with the MP4+AT potential[15] potentials are in excellent agreement with experimental data over the whole ranges of temperatures and pressures.

At a first glance it might be surprising that none of the advanced models [av45z+AT and avtz+(332)+AT] in the present study were able to predict the fluid phase equilibria of neon with sufficient accuracy. It is known, however, that neon shows departure from classical mechanics, and that quantum effects cannot be neglected at low temperatures.[37]

TABLE X. Critical properties of neon.

Potential	T_c/(K)	ρ_c/(kg m^{-3})
cc/avtz+(332)+AT	44.60	484.7
cc/av45z+AT	46.10	493.6
Expt.[a]	44.49	481.9

[a]Reference 36.

For the inclusion of quantum effects in computer simulations several methods have been proposed, e.g., path integral methods[38] or semiclassical simulations based on the Wigner-Kirkwood asymptotic expansion of the partition function in powers of Planck's constant.[39] However, the convergence properties of that expansion are not quite clear, and the path integral method requires significantly larger computational resources. Therefore, we use an equation of state together with a quantum correction function that has been developed to show that the discrepancies in our simulation results of neon are mainly due to quantum effects.

2. Quantum corrections

In quantum fluids, the assumption of continuity of translational energy levels is no longer valid. The discontinuities gain significant influence on thermodynamic properties at low temperatures and high densities for systems containing light atoms or molecules.

Some textbooks of statistical thermodynamics "prove" that translational quantum effects in fluids are insignificant except for liquid helium. This is generally done by comparing the thermal de Broglie wavelength with the intermolecular distance, which in turn is estimated from the liquid density, and observing that the former is almost always significantly smaller.

But this argument is fallacious: The relevant intermolecular distance is not the internuclear distance, but the free path length, which is smaller than the internuclear distance. Consequently, translational quantum effects can occur in all fluids, if only the density is sufficiently high.

Recently, a spherical cell model[40] has been developed to estimate the translational quantum effects in fluids. The model is based on the assumption that each molecule is restricted to a spherical cell formed by its neighbors, with a size depending on the free volume, and that the translational energy levels of the molecule depend on the cell size. The quantum correction function to the molar Helmholtz energy, the deviation of the cell model from the classical limit, can be summarized as

$$\Delta A_m^{qc} = A_m^{quant} - A_m^{class} = -RT(1-e^{-\alpha y^2}) \sum_{i=0}^{13} r_i y^i, \qquad (12)$$

where $y = \Lambda/L$ is a reduced wavelength; the thermal de Broglie wavelength Λ is given by Eq. (6), and L is the cell size (which in turn depends on the free volume),

$$L^3 = \frac{3}{4\pi}\frac{V_f}{N} = \frac{3}{4\pi}\frac{V}{N}\exp\left(-\frac{A_m^{rep}}{RT}\right), \qquad (13)$$

and the r_i are universal expansion coefficients. A_m^{rep} denotes the repulsion part of the molar Helmholtz energy. The model can be applied to any van der Waals type equation of state, i.e., an equation that can be separated into a contribution of repulsive forces and one of attractive forces.

In the present work, the Deiters equation of state (14) (Refs. 41–43) was used to calculate the fluid phase equilibria for neon. It is shown here as equation for the molar Helm-

holtz energy A_m, which contains an ideal gas part, a hard-sphere term with the quantum correction, and an attraction term:

$$A_m = +\mu^{\ominus} - RT\ln\frac{V_m}{V_m^{\ominus}} - RT + RTcc_0\frac{4\xi-3\xi^2}{(1-\xi)^2} + \Delta A_m^{qc} - \frac{N_A}{c^2}\xi\left[h_0\chi(\rho,c)\tilde{T}(e^{1/\tilde{T}}-1) + \sum_{k=0}^{3}\sum_{j=0}^{6}\sum_{i=0}^{10} f_{ijk}(c-1)^k\tilde{T}^{-j}\xi^i\right] \quad (14)$$

with

$$\xi = \frac{N_A\pi\sigma^3}{6V_m}, \quad \tilde{T} = \frac{ck_BT}{\epsilon}.$$

The symbol $\ominus$ refers to the reference state of the equation of state (perfect gas state). The parameters ϵ (potential well depth), σ (hard-core diameter), and c (anisotropy parameter) are substance specific. The f_{ijk} are (universal) expansion coefficients, h_0 and c_0 are constants, $\chi(\rho,c)$ is a function of density, and N_A is Avogadro's constant.

This equation can reproduce pVT and phase equilibrium data of simple fluids over wide ranges of temperatures and pressures. But while the results for the heavier noble gases (argon, krypton, and xenon) are in excellent agreement with experiments, there are deviations from the law of corresponding states for neon and helium arising from quantum effects.

Figures 5 and 6 show the results of the equation of state (with and without the quantum corrections that have been developed), the simulation results of the av45z plus AT potential, and the experimental data for the orthobaric densities and for the vapor pressure. In each case the parameters of the equation of state had been fitted to the critical pressure and temperature. From these figures it can be seen that the agreement of the results of the uncorrected equation of state with experiments especially in the liquid branch is poor, whereas the inclusion of the quantum correction function yields an excellent agreement. On the other hand, there is a fairly good agreement between the results of the uncorrected equation of state and simulation results (av45z+AT). These facts confirm that the discrepancies between results of the simulations and experiments are mainly due to the translational quantum effects.

B. Argon

The av45z potential described in the preceding section was used in GEMC simulations to obtain the vapor pressure and the orthobaric densities of argon. The simulations were performed with and without three-body corrections. The results are displayed in Figs. 7 and 8, as well as listed numerically in the supplementary material.[14]

A comprehensive *ab initio* investigation of three-body nonadditivity effects has been performed recently within the framework of symmetry adapted perturbation theory (SAPT).[44] This theory breaks down the three-body potential into various short-range and long-range components and deals with them separately. In a recent study, Bukowski and Szalewicz[22] analyzed the average contributions of these components to the thermodynamic properties of fluid argon by means of the Gibbs ensemble simulation technique, using the empirical potential of Aziz[24] as two-body potential. Their simulation results are compared with the results obtained here.

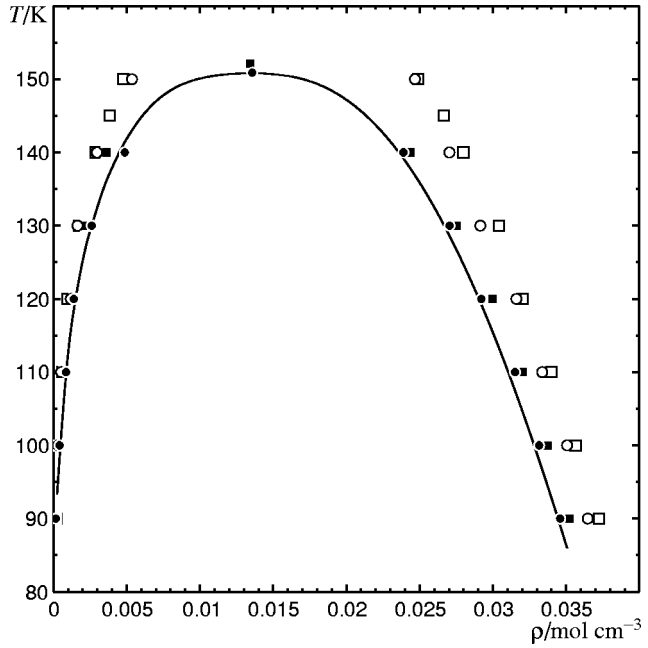

FIG. 7. Densities of coexisting phases of argon. ——, experimental data (Ref. 34). Points, GEMC computer simulation with the following interaction potentials: □, Aziz; ■, Aziz+SAPT; ○, av45z; ● av45z+AT.

The figures show clearly that computer simulations with pair potentials only—empirical or *ab initio*—are not sufficient to reproduce the fluid phase equilibria for argon cor-

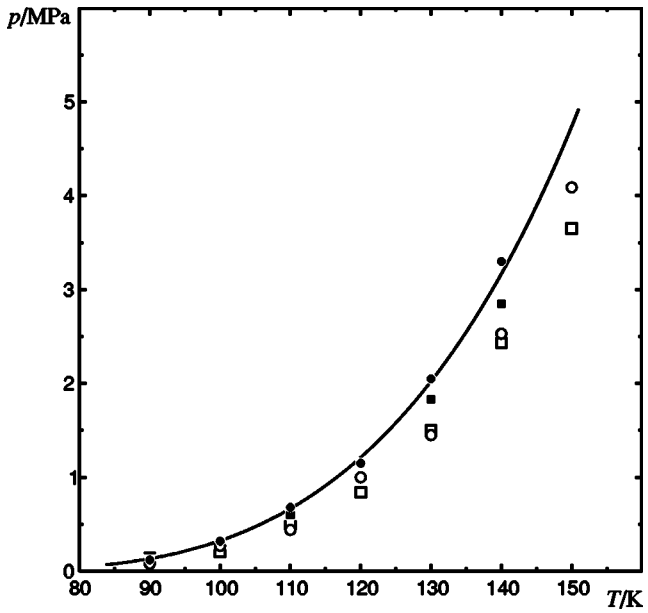

FIG. 8. Vapor pressure of argon. See Fig. 7 for an explanation of the symbols.

TABLE XI. Critical properties of argon.

Potential	$T_c/(\mathrm{K})$	$\rho_c/(\mathrm{kg\ m^{-3}})$
cc/av45z+AT	150.89	542.07
Aziz+SAPT[a]	152.10	536.0
Expt.[b]	150.86	535.6

[a]References 22 and 24.
[b]Reference 36.

rectly. From the same figures it can also be seen that there is a fairly good agreement between our simulation results and those of Bukowski and Szalewicz.[22] As soon as three-body effects are included, either by the AT or the SAPT potential, the simulations achieve a quantitative agreement with the experimental data.

This observation is also confirmed by the recent work of Malijevský and Malijevský,[23] who—with different, but very accurate pair potentials—could quantitatively predict the internal energies and compression factors of argon, krypton, and xenon.

When the critical data of argon were estimated from the phase equilibrium simulations (Table XI), it turned out that the av45z+AT potential (this work) gives an almost exact prediction of the critical temperature, but overestimates the critical density by 1.2%, whereas the Aziz potential[24] enhanced by the SAPT three-body correction yields almost the correct critical density, but overestimates the critical temperature.

These figures confirm that the av45z+AT potential essentially captures the behavior of argon, and that it gives reliable predictions of the fluid phase equilibria of argon. In fact, Bukowski and Szalewicz demonstrated in their simulations that most components of the three-body nonadditivity effect tend to cancel out, and that the remaining difference is very similar to the AT term.

C. Argon-krypton

Simulations were performed with the av45z potential for the argon-argon interaction, the av34z potential for krypton-krypton,[8] and the argon-krypton potential of this work, with and without AT three-body corrections. Phase equilibria were predicted along four isotherms: 158.15, 163.15, 177.38, and 193.15 K. The results of the simulations for two-body potentials are shown in Figs. 9–12; numerical values of the residual chemical potentials, internal energies, densities, and compositions of the coexisting phases can be found in the supplementary material (Tables IX–XIV of Ref. 14).

Qualitatively, the system argon-krypton shows the behavior of a nearly ideal binary mixture. The bubble point curve is almost a straight line over a wide range of compositions. Special computational efforts were needed to reach equilibrium in the critical region. However, as the argon and krypton atoms do not differ much in size, the particle transfer Monte Carlo moves were performed efficiently even at high densities.

Simulations without the AT potential correctly predict the almost ideal behavior of the argon-krypton system, but the phase compositions do not agree well with the experimental data.[45] Again, inclusion of the AT potential leads to a reasonable agreement with experiments at low and moderate pressures. At high pressures, in the vicinity of the (binary) critical points, the agreement deteriorates. But this is a well-known artifact of the simulation technique, caused by large- and wide-ranging fluctuations exceeding the simulation box sizes.

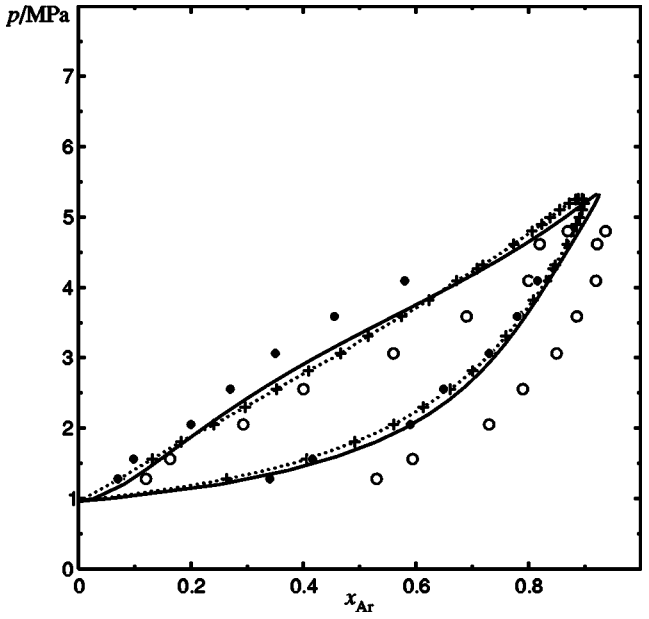

FIG. 9. Isothermal vapor-liquid phase diagram of the system (argon +krypton) at 158.15 K. +, experimental data (Ref. 45); · · · ·, interpolation curve through experimental data (for improved clarity); ○, *ab initio* prediction without three-body potentials; ●, with three-body potentials; –, calculated with equation of state (14) and mixing rules (15) with parameters fitted to *ab initio* prediction with three-body potentials.

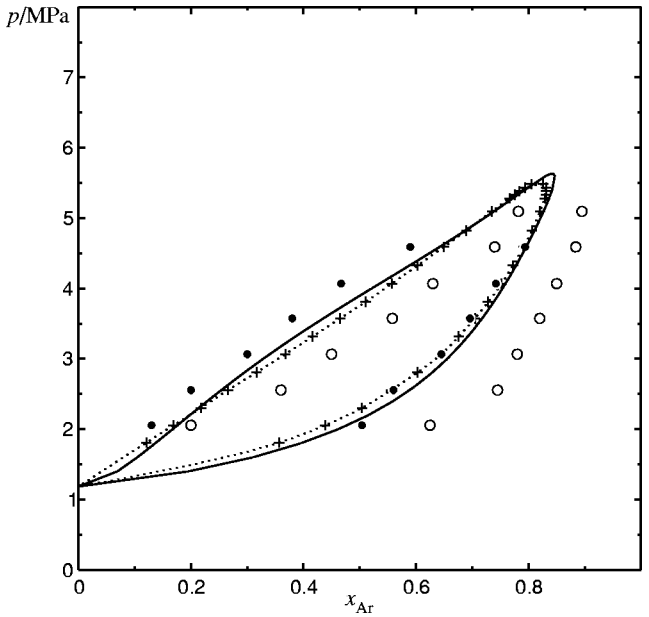

FIG. 10. Isothermal vapor-liquid phase diagram of the system (argon +krypton) at 163.15 K. See Fig. 9 for an explanation of the symbols.

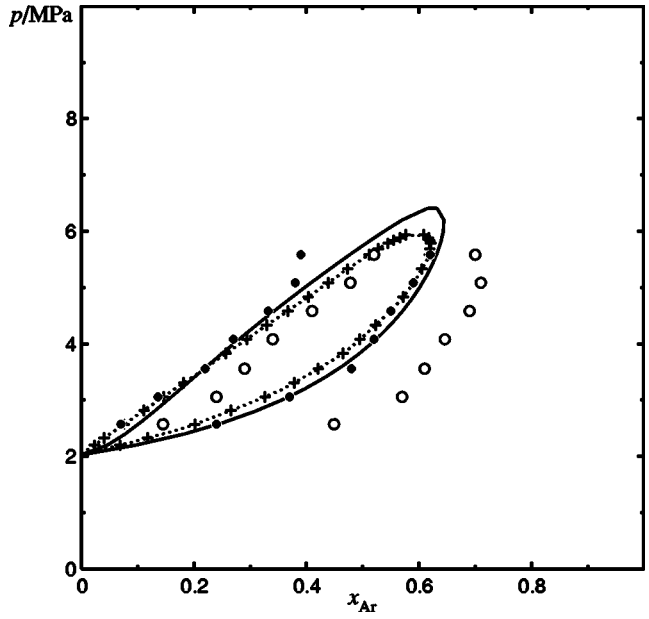

FIG. 11. Isothermal vapor-liquid phase diagram of the system (argon +krypton) at 177.38 K. See Fig. 9 for an explanation of the symbols.

The problem can be circumvented by fitting an equation of state to the predicted equilibrium data (a34z+AT potential) in a pressure range where they are still reliable, and then to extrapolate the high-pressure portion of the phase diagram by solving the thermodynamic equilibrium conditions. Such calculations were performed with the THERMOC program,[46] using again the equation of state (14),[41,42] but with density-dependent mixing rules, which are known to work well for spherical molecules,[47]

$$\epsilon\sigma^{\gamma}=\sum_i \sum_k \epsilon_{ik}\sigma_{ik}^{\gamma},$$

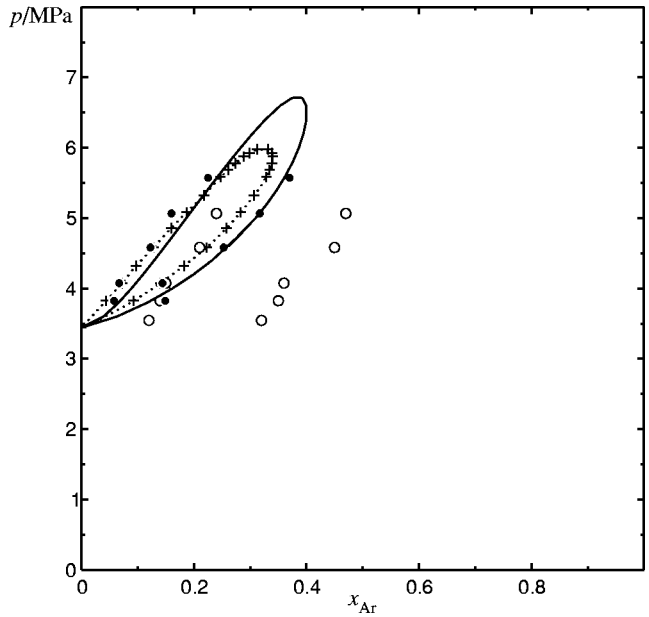

FIG. 12. Isothermal vapor-liquid phase diagram of the system (argon +krypton) at 193.15 K. See Fig. 9 for an explanation of the symbols.

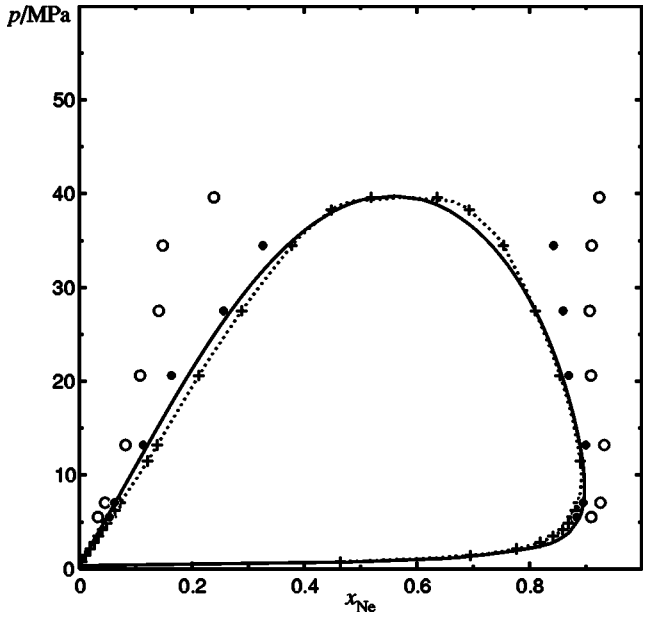

FIG. 13. Isothermal vapor-liquid phase diagram of the system3 (neon +argon) at 101.94 K. +, experimental data Refs. 48 and 49; · · · ·, interpolation curve through experimental data (for improved clarity); ○, *ab initio* prediction without three-body potentials; ●, with three-body potentials; ——, calculated with equation of state (14) and mixing rules (15).

$$\sigma^3=\sum_i \sum_k \sigma_{ik}^3, \tag{15}$$

$$\gamma=3(1-\xi^2).$$

The summations run over the species present in the mixtures. This way it is indeed possible to obtain the complete phase envelope, as well as properties which are notoriously difficult to obtain by computer simulations, e.g., the critical curve, compressibilities, or other higher thermodynamic derivatives.

D. Neon-argon

Simulations were performed with the av45z potential with and without the AT potential along four isotherms: 101.94, 110.78, 121.36, and 129.93 K. The results of the simulations are presented in Figs. 13–16, where they are compared with experimental data;[48,49] numerical simulation results can be found in the supplementary material.[14]

At low temperatures and high pressures much higher computational efforts are needed to reach the equilibrium, because particle transfer trial moves are difficult to perform, especially for the larger atom. Under these conditions and also in the vicinity of critical region, the results of the simulations are very sensitive to the details of the potentials, and the deviations from the experiments increase.

In order to achieve a faster equilibration, the initial compositions in each of the simulation boxes were chosen close to the experimental values. It turned out that, within the usual statistical uncertainty, the results of the simulations were independent of the initial conditions.

Figures 13–16 show a fairly good agreement between simulations based on the av45z potentials and the experi-

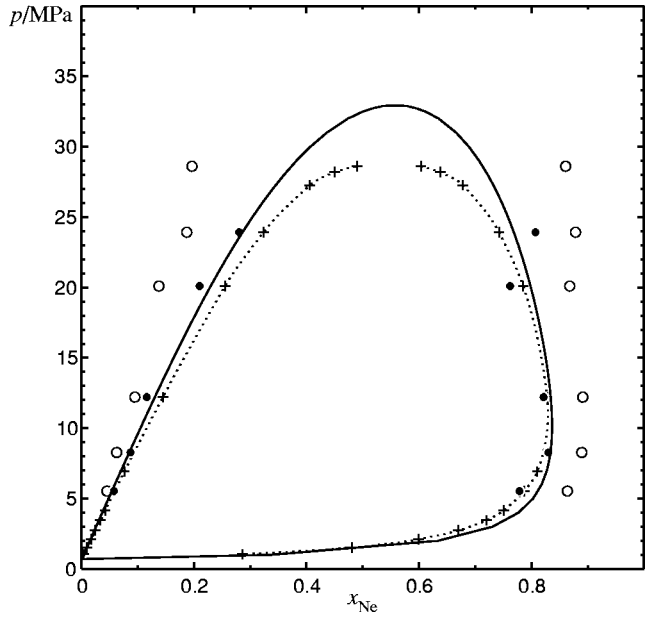

FIG. 14. Isothermal vapor-liquid phase diagram of the system (neon +argon) at 110.78 K. See Fig. 13 for an explanation of the symbols.

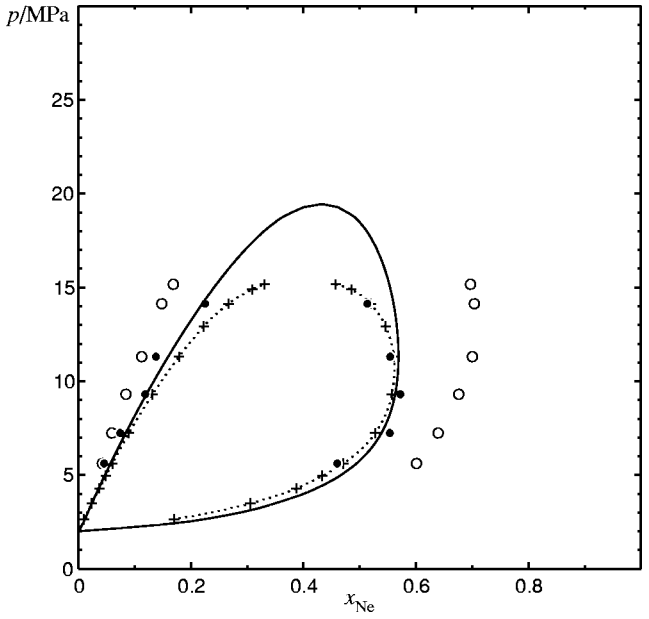

FIG. 16. Isothermal vapor-liquid phase diagram of the system (neon +argon) at 129.93 K. See Fig. 13 for an explanation of the symbols.

ments at low pressures; at higher pressures, however, the deviations increase. The inclusion of the AT potential into the total configuration energy always significantly improves the results.

The same phenomenon had also been observed in the case of pure noble gases; in mixtures, however, it is more pronounced. Far from the critical region the densities of the gas phase in mixtures are much higher than in pure systems, and as a consequence the AT potential contributes more to the configurational energy.

Again it was attempted to fit the simulation results to an equation of state and to calculate the high-pressure portions of the phase diagrams by extrapolation. This approach is successful again, although not with as good an agreement as for (argon+krypton). The reason for this is revealed by Fig. 17, which shows the molar Gibbs energy of the mixture as a function of composition. At elevated pressures, even far away from the binary critical point, the concave regions of the curves are rather shallow, and even a small error in the calculated Gibbs energy can lead to a large shift of the equilibrium compositions. This, however, is a problem not only for computer simulations, but for all calculation methods of high-pressure phase equilibria.

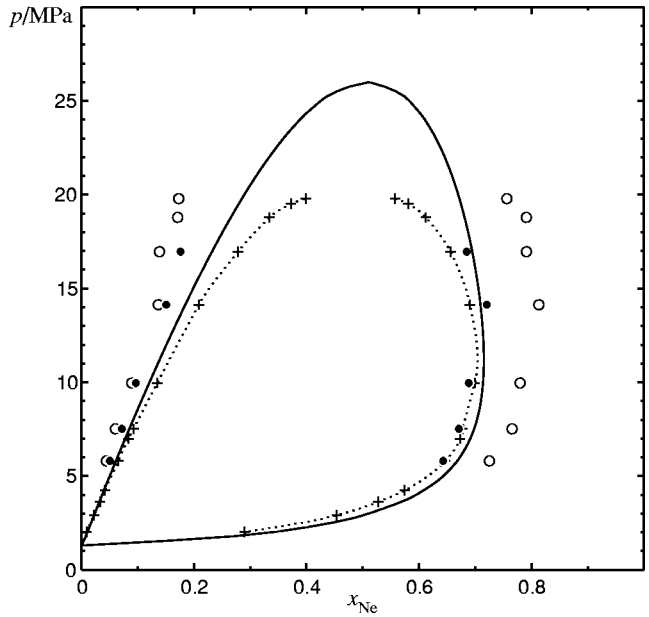

FIG. 15. Isothermal vapor-liquid phase diagram of the system (neon +argon) at 121.36 K. See Fig. 13 for an explanation of the symbols.

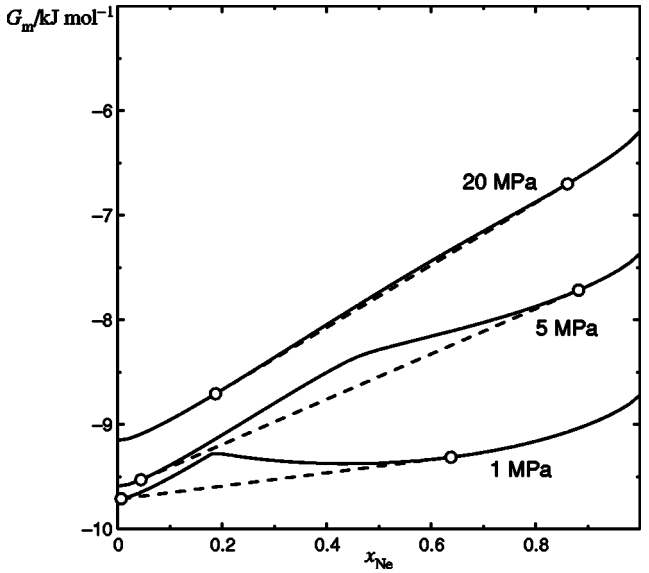

FIG. 17. Gibbs energy of the system (neon+argon) at 101.94 K for various pressures. ——, calculated with the equation of state (14); — — —, double tangent; ○, phase equilibrium compositions.

V. CONCLUSION

Quantum mechanical calculations by means of the coupled-cluster technique, performed at the CCSD(T) level and with correlation-consistent basis sets are able to yield pair potentials, which can be used in computer simulations to predict thermodynamic properties of fluids. In order to achieve quantitative agreement with experiment, it is necessary to account for three-body effects by means of the AT potential. Thus we can report successful ''global simulations'' (predictive computer simulations without recourse to experimental data except for some universal constants) for argon and—citing previous work—krypton. For neon quantum corrections are necessary for a quantitative description of its vapor pressure curve and the coexisting phase densities.

We extended the global simulations to the calculation of high-pressure vapor-liquid phase equilibria of the *mixtures* (neon+argon) and (argon+krypton); for the latter system a pair potential has been developed in this work. The calculation of such phase equilibria at high pressure, which involve binary critical points and retrograde behavior, is usually not a trivial task. It turns out that the simulations presented here are able to predict a large part of the phase envelope; the gaps (which are due to systematic limitations of the simulations) can be bridged efficiently by an equation of state. Hence it is possible to fully predict the high-pressure phase diagrams of the noble-gas mixtures (neon+argon) and (argon +krypton).

ACKNOWLEDGMENTS

The Regional Computer Center of Cologne (RRZK) contributed to this project by a generous allowance of computer time as well as by efficient software support; we especially wish to thank Dr. L. Packschies (RRZK) for technical help with quantum mechanical software. This work was financially supported by the Fonds der Chemischen Industrie e.V.; furthermore, support by INTAS (Project No. 640-00) is gratefully acknowledged.

[1] A. Z. Panagiotopoulos, Mol. Phys. **61**, 813 (1987).
[2] D. A. Kofke, Adv. Chem. Phys. **105**, 405 (1999).
[3] A. Z. Panagiotopoulos, J. Phys.: Condens. Matter **12**, R25 (2000).
[4] R. Eggenberger, S. Gerber, H. Huber, and M. Welcker, Mol. Phys. **82**, 689 (1994).
[5] B. Kirchner, E. Ermakova, J. Solca, and H. Huber, Chem.-Eur. J. **4**, 383 (1998).
[6] S. L. Garrison and S. I. Sandler, J. Chem. Phys. **117**, 10571 (2002).
[7] K. Leonhard and U. K. Deiters, Mol. Phys. **100**, 2571 (2002).
[8] A. E. Nasrabad and U. K. Deiters, J. Chem. Phys. **119**, 947 (2003).
[9] P. E. S. Wormer and A. van der Avoird, Chem. Rev. (Washington, D.C.) **100**, 4109 (2000).
[10] G. Chałasiński and M. M. Szczęsniak, Chem. Rev. (Washington, D.C.) **100**, 4227 (2000).
[11] S. M. Cybulski and R. R. Toczyłowski, J. Chem. Phys. **111**, 10520 (1999).
[12] W. Klopper, Mol. Phys. **99**, 481 (2001).
[13] R. A. Aziz and M. J. Slaman, Chem. Phys. **130**, 187 (1989).
[14] See EPAPS Document No. E-JCPSA6-121-516434 for tabulations of the pair potentials and numerical results of the computer simulations. A direct link to this document may be found in the online article's HTML reference section. The document may also be reached via the EPAPS homepage (http://www.aip.org/pubservs/epaps.html) or from ftp.aip.org in the directory /epaps/. See the EPAPS homepage for more information.
[15] K. Leonhard and U. K. Deiters, Mol. Phys. **98**, 1603 (2000).
[16] T. Korona, H. L. Williams, R. Bukowski, B. Jeziorski, and K. Szalewicz, J. Chem. Phys. **106**, 5109 (1997).
[17] K. T. Tang and J. P. Toennies, J. Chem. Phys. **80**, 3726 (1984).
[18] M. Venkatraj, C. Bratschi, H. Huber, and R. J. Gdanitz, Fluid Phase Equilib. **218**, 285 (2004).
[19] J. O. Hirschfelder, C. F. Curtiss, and R. B. Bird, *Molecular Theory of Gases and Liquids* (Wiley, New York, 1954).
[20] G. Grochola, S. Russo, and I. Snook, Mol. Phys. **95**, 471 (1998).
[21] B. M. Axilrod and E. Teller, J. Chem. Phys. **11**, 299 (1943).
[22] R. Bukowski and K. Szalewicz, J. Chem. Phys. **114**, 9518 (2001).
[23] A. Malijevský and A. Malijevský, Mol. Phys. **101**, 3335 (2003).
[24] R. A. Aziz, J. Chem. Phys. **99**, 4518 (1993).
[25] *Thermodynamic Tables–NonHydrocarbons*, edited by K. R. Hall (Thermodynamic Research Center, Texas, 1972).
[26] D. A. Barrow and R. A. Aziz, J. Chem. Phys. **89**, 6189 (1988).
[27] O. Shamma and M. Rigby, J. Chem. Soc., Faraday Trans. **78**, 689 (1982).
[28] A. Kumar and W. J. Meath, Mol. Phys. **54**, 823 (1985).
[29] S. F. Boys and F. Bernardi, Mol. Phys. **19**, 553 (1970).
[30] J. Kestin, K. Knierim, E. A. Mason, B. Najafi, S. T. Ro, and M. Waldman, J. Phys. Chem. Ref. Data **13**, 229 (1984).
[31] I. A. McLure, J. E. Ramos, and F. del Río, J. Phys. Chem. B **103**, 7019 (1999).
[32] J. H. Dymond and E. B. Smith, *The Virial Coefficients of Pure Gases and Mixtures* (Clarendon, Oxford, 1980).
[33] M. P. Allen and D. Tildesley, *Computer Simulation of Liquids* (Clarendon, Oxford, 1987).
[34] *Landolt-Börnstein Zahlenwerte und Funktionen*, edited by K. Schäfer and E. Lax (Springer, Berlin, 1960), Vol. II/2a.
[35] D. Frenkel and B. Smit, *Understanding Molecular Simulation*, 2nd ed. (Academic, London, 2001).
[36] N. B. Vargaftik, *Tables on the Thermophysical Properties of Liquids and Gases in Normal and Dissociated States* (Wiley, New York, 1975).
[37] L. M. Sese, Mol. Phys. **78**, 1167 (1993).
[38] K. Singer and W. Smith, Mol. Phys. **64**, 1215 (1988).
[39] J. P. Hansen and J. J. Weis, Phys. Rev. A **36**, 2440 (1987).
[40] R. Laghaei, Ph.D. thesis, University of Cologne, 2003.
[41] U. K. Deiters, Chem. Eng. Sci. **36**, 1139 (1981).
[42] U. K. Deiters, Chem. Eng. Sci. **36**, 1146 (1981).
[43] U. K. Deiters, Chem. Eng. Sci. **37**, 855 (1982).
[44] V. F. Lotrich and K. Szalewicz, J. Chem. Phys. **106**, 9688 (1997).
[45] J. A. Schouten, A. Deerenberg, and N. J. Trappeniers, Physica A **81**, 151 (1975).
[46] U. K. Deiters, Chem. Eng. Technol. **23**, 581 (2000).
[47] U. K. Deiters, Fluid Phase Equilib. **33**, 267 (1987).
[48] W. B. Streett, J. Chem. Phys. **42**, 500 (1965).
[49] W. B. Streett, J. Chem. Phys. **46**, 3282 (1967).
[50] J. A. Anta, E. Lomba, and M. Lombardero, Phys. Rev. E **55**, 2707 (1997).
[51] E. Ermakova, J. Solca, G. Steinebrunner, and H. Huber, Chem.-Eur. J. **4**, 377 (1998).
[52] R. A. Aziz and M. J. Slaman, Mol. Phys. **58**, 679 (1986).